A Pan-European high resolution storm surge hindcast

T. Fernández-Montblanc[a,*], M.I. Vousdoukas[b], L. Mentaschi[b], P. Ciavola[a]

[a] Universitá degli Studi di Ferrara, Department of Physics and Earth Sciences, Via Saragat, 1. 44122 Ferrara, Italy
[b] European Commission, Joint Research Centre (JRC), Via Enrico Fermi 2749, I-21027 Ispra, Italy

ARTICLE INFO

ABSTRACT

This contribution presents the high-resolution Pan-European storm surge (SSL) dataset, ANYEU-SSL, produced with the SCHISM circulation model. The dataset covers 40 years (1979–2018) of SSL data along the European coastline with 3-hour temporal resolution and has been extensively validated for the period spanning from 1979 to 2016, considering the whole time series, as well as for the extreme SSL values. Validation against tidal gauge data shows an average RMSE of 0.10 m, and RMSE below 0.12 m in 75% of the tidal gauges. Comparisons with satellite altimetry data show average RMSE of 0.07 m. SSL trends are estimated as an example of a potential application case of the dataset. The results indicate an overall latitudinal gradient in the trend of the extreme storm surge magnitude for the period 1979–2016. SSLs appear to increase in areas with latitudes > 50 °N and to decrease in the lower latitudes. Additionally, a seasonal variation of the extreme SSL, particularly strong in the northern areas, has been observed. The dataset is publicly available and aspires to provide the scientific community with an important data source for the study of storm surge phenomena and consequential impacts, either on large or local scales.

1. Introduction

Coastal inundation is considered one of the most damaging natural disasters, causing casualties and significant economic losses (Hinkel et al., 2014). Particularly, storm surge is a major coastal flooding driver (Resio and Westerink, 2008). Surges constitute a temporary increase in sea level that persists for several hours and cannot only cause coastal inundation, but also increase the wave driven hazard, i.e. erosion (Shaw et al., 2016; Smith et al., 2010) and coastal protection failure (Hatzikyriakou and Lin, 2017; Oumeraci, 1994). Moreover, sea levels have been rising and will continue to do so (Bamber et al., 2019; Jevrejeva et al., 2016), which along with changes in wind and pressure systems (Elsner et al., 2008; Hemer et al., 2013; Vousdoukas et al., 2018a, 2018b; Vousdoukas et al., 2017; Wahl et al., 2017) will increase future coastal risks (Hinkel et al., 2014; Vousdoukas et al., 2018a, 2018b). Given that weather patterns vary at time scales ranging from hours to decades, having high quality time series which span several decades is essential for most studies concerning the dynamics of extreme sea levels (Haigh et al., 2016). In addition it is very important for policy making and the design of adaptation policies especially in view of climate change.

Extreme value analysis and temporal-spatial variability of extreme sea levels were traditionally based on tidal gauge data (Haigh et al., 2016; Menéndez and Woodworth, 2010; Tsimplis and Blackman, 1997). However, in situ measurements come with limitations in terms of spatial and temporal coverage. Measurement networks are spatially sparse and tidal gauges are usually moored in sheltered locations, such as estuaries or harbours, where the conditions and complex bathymetry often make them not representative for the wider area. In addition, in situ measurements often include errors, irregular sampling and data gaps (Cid et al., 2014), and the latter often coincide with the extreme events that matter. Alternative sea level data sources, such as altimetry satellite measurements, are free of spatial limitations; however, they are characterized by low temporal resolution. In addition, the uncertainty associated with satellite-based measurements increases in coastal zones where the satellite footprint includes both land and ocean (Cipollini et al., 2017).

With respect to the above-mentioned limitations of other data sources, numerical models have become established as a valid alternative (Bertin et al., 2013; Camus et al., 2013; Chawla and Spindler, 2013; Menendez et al., 2014; Muis et al., 2016), showing clear advantages in terms of temporal and spatial resolution and providing adequate temporal coverage to resolve also long term variations. Typically, numerical models are validated against in situ measurements for the period when there is overlap, and following they are used to fill data gaps and extend the dataset spatially or temporally. In addition,

Table 1
Examples of hydrodynamic hindcasts of publicly available meteorological residual datasets.

Reference	Time range	Domain	Atmospheric forcing	Ocean model	Ocean model resolution
Sebastião et al. (2008) (HIPOCAS)	1958–2001	North Eastern Atlantic	REMO (0.5 × 0.5)	HAMSO	10′ × 15′
Cid et al. (2014) GOS 1.1 and GOS 2.1	1948–2009 1989–2009	Southern Europe	SeaWindI 30 km SeaWindII 15 km	ROMS	1/8 × 1/8
Ratsimandresy et al. (2008)	1958–2001	Mediterranean Sea	REMO (0.5 × 0.5)	HAMSO	10′ × 15′
Hamon et al. (2016)	1979–2013	Mediterranean sea	ALDERA 12 km	NEMO	6–7.5 km
Jordà et al. (2012) VANI2-ERA	1950–2008	Mediterranean Sea North eastern Atlantic	ARPERA (40–50 km)	HAMSO	10′ × 15′
https://www.bodc.ac.uk/resources/inventories/edmed/ report/755/'	1955 onwards	NW European continental shelf North east Atlantic	DNMI (75 km)		35 km
Weidemann (2015) coastDat-2_TRIM-NP-2d-Baltic	1958–2011	Baltic Sea		NP V2.1	12.8–6.4–3.2–1.6 km
Weidemann (2015) coastDat-2 TRIM-NP-2d	1948–2015	North Sea and Northeast Atlantic		NP V2.1	

reanalysis data can be analysed using similar techniques to the case of observational record and there are several examples of storm surge analyses; e.g. on the long term variations and trends in storm surges (Cid et al., 2015), projections of extreme storm surges (Paprotny et al., 2016; Vousdoukas et al., 2017), storm surge variation associated to climate changes (Butler et al., 2007; Calafat et al., 2014), and flood exposure (Muis et al., 2017). Table 1 gives examples of previous hindcast which also resulted in public datasets. As indicated in table the spatial and temporal coverage, as well as spatial resolution of previous efforts is quite variable and there is an absence of high-resolution datasets (i.e. < 25 km) covering the Pan-European area. Some high resolution storm surge hindcasts are available e.g. one based on numerical modelling for the Iberian Peninsula (Fortunato et al., 2016) and one from statistically reanalysis for the North Sea (Dangendorf et al., 2014). Moreover, there are several studies assessing the effect of climate change scenarios on future storm surges along different European areas: the Mediterranean Sea (Androulidakis et al., 2015; Conte and Lionello, 2013), Southern Europe (Marcos et al., 2011), North Sea (Woth et al., 2006), Baltic Sea (Meier, 2006). However, aggregating or comparing at continental scale is impeded by the fact that all studies include a reanalysis spanning along a different baseline period, highlighting once more the need for a Pan-European storm surge reanalysis.

The present work aims at assessing SSL variability along European coasts and its trends based on the ANYEU-SSL, a high-resolution hindcast of the meteorological (wind and pressure driven) water level component; hereafter non-tidal residual (NTR) refers to the whole time series, whereas the storm surge level (SSL) corresponds to the upper tail distribution (> 95th percentile) of the non-tidal residual. The ANYEU SSL is a Pan-European hindcast; it was generated using a cross-scale ocean circulation model covering the area between longitudes 25 W to 42E and latitudes 25 N to 76 N (see: thick black line in Fig. 1). ANYEU-SSL is a long-term storm surge dataset, spanning from 1979 to 2018, while its variable spatial resolution ranges from ~70 km up to 10 km, and its temporal resolution is 3-hours. This study is organised as follows. Section 2 is mainly devoted to presenting the model setup and validation, as well as other methodological aspects. Section 3 presents results from the validation as well as the analysis of spatial and temporal storm surge dynamics. Finally, concluding remarks are summarised in Section 4.

2. Methods

2.1. Model setup

Surge generation and propagation has been simulated using the SCHISM model (Semi-implicit Cross-scale Hydroscience Integrated System Model), which is based upon the original SELFE code v3.1dc (Zhang and Baptista, 2008), albeit with many enhancements and upgrades, including an extension to a large-scale eddying regime and a seamless cross-scale capability from creek to ocean (Zhang et al., 2016).

The model solves the full Navier-Stokes equations for an unstructured mesh with triangular elements and varying resolution ranging from ~70 km on the far coast of Greenland to 10 km in European shallow coastal areas. The SCHISM model is used in its 2D barotropic mode and was forced by the meteorological fields (10 m wind speed and sea level pressure) based on ERA-Interim re-analysis from the European Centre for Medium-range Weather Forecast (ECMWF), with 0.75° × 0.75° horizontal resolution and 6 h temporal resolution. The wind surface stress was computed using a bulk formula with the drag coefficient calculated according to Pond and Pickard (2013). The bed shear stress was computed using the Manning approach, assuming a value of 0.02 for the Manning friction coefficient. A viscosity filter with a diffusion-number-like dimensionless constant of 0.025 is used to suppress inertial spurious modes (grid-scale noises) (Zhang et al., 2016).

The bathymetry dataset was obtained from the European Marine Observation and Data Network (EMODnet) in angular coordinates at a resolution of 1/8 arc-minute (0.0021° of latitude and longitude) (http://www.emodnet.eu/bathymetry) and were interpolated onto the computational grid.

The model simulations were conducted separately for each year. Each run covered 13 months using the first month as spin-up time. A detailed description of the model setup can be found in Fernández-Montblanc et al. (2019).

2.2. Assessment of hindcast performance

2.2.1. Validation against tide gauge data

The model was validated against water level time series available from two databases: the JRC Tidal Gauge Database (http:// webcritech. jrc.ec.europa.eu/SeaLevelsDb), and the EMODnet web site database (http://www.emodnet-physics.eu/Map/). The validation period spanned from 01/02/1979 to 31/12/2016.

The tidal gauge sea level measurements were pre-processed to remove errors and irregular sampling periods. The time series were detrended on a yearly basis to remove long-term mean sea level variability. Afterwards, a tidal harmonic analysis was performed using the t-tide package (Pawlowicz et al., 2002), separating the astronomical tide and the non-tidal residual (η_{RE}) components. Although η_{RE} includes the atmospheric contribution and the non-linear tidal-surge (Haigh et al., 2016), it was compared with the SSL registered in the nearest model's mesh node.

The model skill of the hindcast to reproduce the measured SSL was evaluated using the root mean square error (RMSE) (Eq. (1)), relative root mean squared error (%RMSE) (Eq. (2)) and Pearson correlation coefficient (r) (Eq. (3)).

$$RMSE = \sqrt{\frac{\Sigma_k^n (\eta_o^k - \eta_p^k)^2}{n}}$$
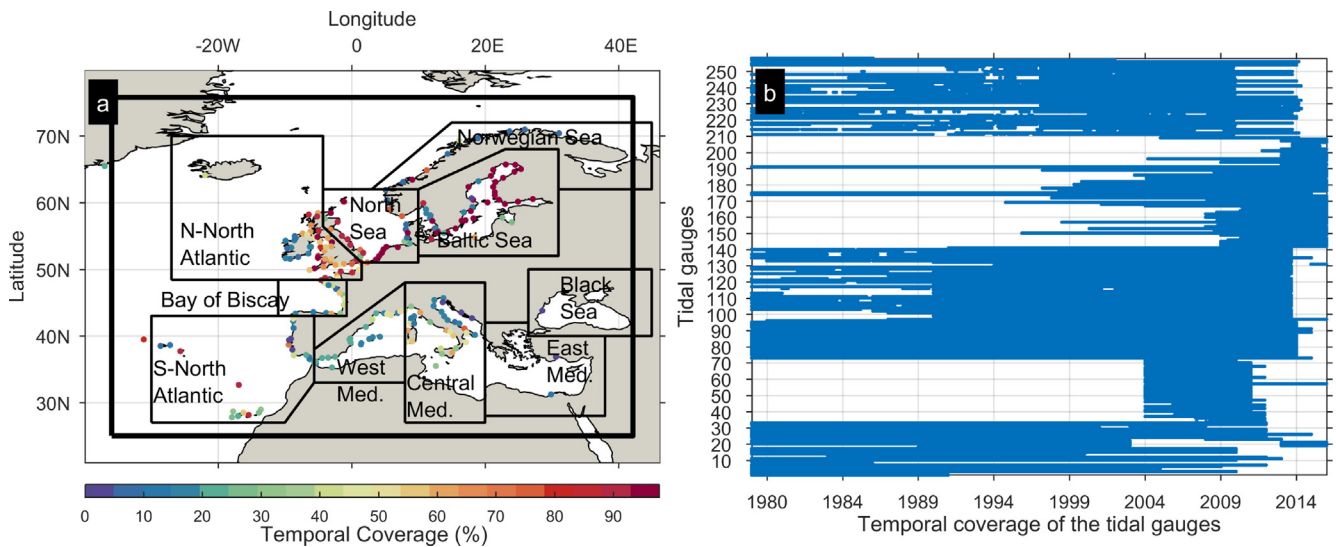
$$(1)$$

Fig. 1. (a) Map of Europe showing the model computational domain (thick black line), the 10 different regions chosen for analysing the model results (thin continuous black lines), and the location of tide gauge stations (the colour scale indicates the temporal coverage of the data as a percentage of the validation period from 1979 to 2016. (b). Time line coverage of the various tide gauge data during the validation period. (For interpretation of the references to colour in this figure legend, the reader is referred to the web version of this article.)

$$\%RMSE = \frac{\sqrt{\frac{\Sigma_k^n(\eta_o^k - \eta_p^k)^2}{n}}}{\max(\eta_o)} \cdot 100 \tag{2}$$

$$r = \frac{\Sigma_i^n(\eta_o^k - \overline{\eta_o^k})}{\sqrt{\Sigma_i^n(\eta_o^k - \overline{\eta_o^k})^2}\sqrt{\Sigma_i^n(\eta_p^k - \overline{\eta_p^k})^2}} \tag{3}$$

where n is a number of measurements in the time series at a given location, η_o is the observed storm surge, η_p is the predicted storm surge.

The accuracy of the model to reproduce extreme storm surge events was evaluated only for the tide gauge stations with time series records covering at least 10 years, where measured and modelled extreme SSL were compared. In those stations, an extreme value analysis was carried out based on a Peak-Over Threshold (POT) approach (Mentaschi et al., 2016). The extremes were selected considering the 95th percentile as threshold, which ranges from 0.05 to 0.86 m, and a 3-day time window to separate independent events. Extreme event exceedance was modelled according to the Generalized Pareto Distribution (GPD). The BIAS between the hindcasted extreme SSL and extreme SSL measured by tidal gauges was calculated for 1 (BIAS RP1) and 10 (BIAS RP10) year return levels.

2.2.2. Validation against satellite altimetry data

Additional validation against a satellite altimetry dataset took place as (i) it allowed to assess areas where tide gauge databases show limitations in spatial and temporal coverage, e.g. along the Eastern Mediterranean or the Black Sea; (ii) it allowed to validate the model in open ocean areas not covered by tidal gauges. The used altimeter dataset was the GLOBAL OCEAN ALONG-TRACK L3 SEA SURFACE HEIGHTS REPROCESSED from CMEMS (Copernicus Marine Environment Monitoring Service) (http://marine.copernicus.eu). This product was processed by the DUACS multimission altimeter data processing system (http://duacs.cls.fr) to even out all available altimeter missions (Topex-Poseidon; Topex-Poseidon (interleaved orbit); Jason-1; Jason-1 (interleaved orbit); Jason-1 (geodetic orbit); OSTM/Jason-2; OSTM/Jason-2 (interleaved); Jason-3; Sentinel-3A; ERS-1; ERS-2; Envisat; Envisat (extended phase); Geosat Follow On; Cryosat; SARAL/AltiKa; SARAL-DP/ALtiKa; HY-2A; HY-2A (geodetic orbit)). The spatial resolution is 14 km and the temporal resolution varies from 10 to 35 days depending on the satellite. The resultant Sea Level Anomaly (SLA) includes different corrections in order to reduce instrumental

miscalculations as well as environmental, state, and geophysical errors (geoid, ocean tide, inverse barometer and high frequency wind and pressure effects). In the derived SLA, the inverse barometer and high-frequency wind signal of the atmospheric forcing was removed through the so-called Dynamic Atmospheric Correction (DAC) produced by CLS using the Mog2D model from Legos distributed by Aviso+, with support from CNES (https://www.aviso.altimetry.fr/). The DAC was rendered as a linear addition to the SLA in order to include all atmospheric forcing contributions to the sea level variation (SLA_{DAC}).

Afterwards, SLA_{DAC} was compared with the SSL hindcast. To that end, the computational domain was gridded into $1° × 1°$ latitude and longitude cells. The time series of the along track SLA_{DAC} was constructed for each $1° × 1°$ cell and modelled data were interpolated in time and space to match the altimeter dataset. Skill scores identical to one used fot tide gauge comparison (RMSE, %RMSE and r) were used in the case of the altimeter observation dataset. For the extreme SSL assessment, the comparison was performed using the same skill scores calculated for the upper tail distribution (> 95th). The validation period for the altimeter observations was expanded from 1992 to 2016, a period also covered by most of the tide gauge record (Fig. 1b).

2.3. Application example: Trends in extreme SSL

In order to demonstrate the utility of the present dataset, the ANYEU-SSL was used to evaluate spatial variability of the extreme storm surge trends at Pan-European scale. The trends in extreme SSL along the European coastline were calculated for the period of the hindcast dataset validated with tidal gauges and altimetry measurements, from 1979 to 2016. A non-stationary extreme value analysis was carried out, consisting of the transformation of a non-stationary time series into a stationary one, where extreme value analysis theory can be applied and reverse the transforming result into a non–stationary extreme value distribution (Mentaschi et al., 2016). The transformed-stationary methodology was applied with a time window of 6 years, considering a 3-day time window as an independent event to estimate a non-stationary GPD, see Mentaschi et al. (2016) for further details. The SSL trends were expressed as the result of the linear regression fitting of the extreme SSL corresponding to the return period (T_r) for $T_r = 10$ and $T_r = 100$. The locations where the trend's statistical significance was lower than 99.5% (p-value > 0.05) were discarded. Following the same methodology, seasonal variability of extreme storm surge trends

have been tested by repeating the analysis for winter (spanning from December to February), spring (from March to May), summer (from June to August) and autumn (from September to November).

3. Results and discussion

3.1. Validation against tidal gauges

The tide gauge database used for the ANYEU-SSL validation contains 258 stations. After an initial filtering of the tide gauge records, a total of 252 stations were used for the hindcast dataset validation. The spatial and temporal coverage of the tide gauge database is shown in Fig. 1. Overall, the Pan-European coastline is uniformly covered and well represented by the tide gauges (Fig. 1a). The Baltic and North Seas show a high density of tide gauge stations, while the coverage is lower along the Black Sea and East Mediterranean. Temporal coverage is higher in the Baltic, North Sea and N-North Atlantic (70–100% of the 1979–2016 period) than in the southern part of the computational domain (< 50%) (Fig. 1a). However, most of the tidal gauge station measurements are available after 2007 (Fig. 1b), a period characterized by substantial marine storm activity, implying sufficient amount of validation data (Bertin et al., 2012; Haigh et al., 2016; Spencer et al., 2015).

Fig. 2 shows examples of the time series comparison for the different ocean regions. The set of examples illustrates areas characterised by a wide range of extreme SSL; see, for example, the maximum SSL of 1.5 m measured in Ijmuiden (Fig. 2c) in the North Sea and 0.3 m measured in Ibiza, in the Central Mediterranean (Fig. 2f). Minor discrepancies > 0.05–0.1 m can be observed in most of the time series for the NTR. The Eastern Mediterranean, represented by the Alexandria station (Fig. 2g), shows the poorest performance. The differences in the extreme SSL between measurements and hindcast dataset ranges from 0.10 to 0.25 in most of the computational domain. The dissimilarities relative to the observed maximum are lower in the areas with a higher extreme SSL (Fig. 2a-d). Overall, the hindcast shows satisfactory skill both in terms of NTR amplitude and timing, but an underestimation of the extremes SSL.

Fig. 3 illustrates the hindcast's capacity to reproduce the probability distribution functions of the observed NTR at different oceanographic regions, using q-q plots. Bearing in mind that the selected stations were mostly different from those shown in Fig. 2, the hindcast in these stations, shows good agreement with the observed data too, either in terms of NTR magnitude (RMSE < 0.1 m) or timing (r around ∼ 0.8). In general, the hindcast reproduces the distribution of observed data (NTR) with some exceptions for the tails. The lower tails are not so important in terms of coastal risk, but they are well reproduced, with the exception of an overestimation observed mainly in the southern seas of Europe (Black Sea, Central and Eastern Mediterranean; see Fig. 3k-m). Regarding the upper tail (SSL), the model performs well in most stations, with the exception of the S-North Atlantic (Gijon and Sines, Fig. 3g and Fig. 3h, respectively), West Mediterranean (Mahon, Fig. 3c), East Mediterranean (Alexandria, Fig. 3i) and Black Sea (Mangalia, Fig. 3m). Overall, the model performance is considered satisfactory, and the underestimation observed at certain locations can be justified by the model's and atmospheric forcing resolution.

Fig. 4 shows scatter plots of different model skill scores (RMSE, % RMSE and r) after comparison against tide gauge data. Overall, the hindcast shows a good skill with RMSE ranging from 0.04 to 0.24 m (Fig. 4a, Table 2). RMSE values below 0.12 m are observed in 80% of the tide gauge stations, while RMSE values above 0.17 m are found in 5.6% of the model domain (Fig. 4b). The average RMSE along all considered European regions is below 0.11 m, with the exception of the North Sea and the Baltic Sea, where the average RMSE values are around 0.12 m and 0.14 m, respectively. The %RMSE varies from 1% to 30% (Fig. 4c, Table 2), however %RMSE < 12.5 is observed in most of the tide gauges (69%) (Fig. 4d). On the contrary, %RMSE > 15% is

recorded only in 11% of the considered tidal gauges; with the highest values found mainly the Mediterranean Sea, following opposite patterns to the RMSE trends.

Pearson coefficients r also indicate a satisfactory model's skill to reproduce temporal correlations, with values $0.6 < = r < = 0.9$ (Fig. 4e, Table 2) along all European regions. The correlation coefficient exceeds 0.7 in more than 72% of the analysed tide gauges, whereas only 7% of the tide gauge stations show values of r < 0.5. Overall, r > 0.7 can be observed in the whole domain, with the exception of the Canary Islands, the Central and Western Mediterranean and the Black Sea.

The validation of the upper tail values (SSL) (Fig. A1) shows values of RMSE ranging from 0.05 to 0.5 m; however, for > 87% of the tidal gauges RMSE lies between 0.05 and 0.2. The higher values (RMSE = 0.2–0.3 m) were observed in the North Sea, according to the higher extremes measured in that area. The %RMSE ranges from 5 to 20% in more than 72% of the analysed stations. Higher values (> 30%) were observed in the Central Mediterranean and southern North-Atlantic border. Regarding the timing of the SSL, correlation coefficients vary between 0.5 and 0.7 in more than 50% of the tidal station. Lower r values were observed in the central Mediterranean and southern S-North Atlantic.

Validation focussing on the extreme SSL values showed an overall satisfactory performance (Fig. 5a–e), especially along the North and Baltic Sea where SSLs tend to be higher. Discrepancies are higher for the higher return period events (Fig. 5f). There is a general trend to underestimate extreme SSLs for $T_r > 10$ years, reaching discrepancies values of 0.2–0.3 m at some stations. This trend is especially relevant along the southern part of the computational domain, but it can be also observed at some locations in Northern Europe (Fig. 5a, Fig. 5f). Larger deviations are also observed along the Southern Atlantic border (Fig. 5g), and the Central and Eastern Mediterranean (Fig. 5j–k); however, the magnitude of the extreme SSL is significantly lower.

Fig. 6 shows the absolute error of modelled extreme SSL validation against tidal gauge data. In most stations the hindcast satisfactorily reproduces the extreme SSL; although, a general underestimation pattern is identified in both the 1 year return period (BIAS RP1) (Fig. 6a) and the 10 year return period (BIAS RP1) (Fig. 6c). The average absolute values of BIAS RP1 and BIAS RP10 are below 0.13 and 0.20 m, respectively, along most European regions (Table 3), while absolute errors range from −0.1 m to 0.1 m in 37% and 28.6% for RP1 (Fig. 6b) and RP10 (Fig. 6d), respectively. A larger BIAS (from −0.2 to 0.1) is detected in 36.1% of the tide gauges for RP1 and 28.6% for RP10. The largest underestimation (BIAS RP1 and BIAS RP10 < 0.2 m) is observed along the Northern Adriatic, the North Sea, and the Bay of Biscay. On the contrary, the hindcast overestimates the RP1 and RP10 in the English Channel and the Central Mediterranean.

3.2. Validation against satellite altimetry measurements

The SSL from satellite altimetry (SLA_{DAC}) allows validating the ANYEU-SSL dataset throughout the whole computational domain, also compensating for spatial limitations of the tide gauge database. Fig. 7 depicts the scatter plots and q-q plots for the $1° \times 1°$ cell closest to the tide gauge station presented in Fig. 3. The hindcast shows a good performance in most of the locations, as well as better skill scores in magnitude (RMSE) or timing (r) with respect to the tide gauge validation (Fig. 3) for the NTR validation. A narrow distribution of the scatter points around the perfect fit line ($\eta_o = \eta_p$) can also be observed. However, at specific locations (see Fig. 7d or Fig. 7f) the calculated RMSE increases by 3–4 cm with respect to the RMSE computed from the tide gauge record. Considering the upper and lower tail distribution, the q-q plot shows a poorer performance than the tide gauge validation. The non-alignment of the lower and higher percentiles with the perfect fit line indicate that the hindcast underestimates the upper tail and overestimates the lower tail values, even if the lowest frequency satellite data are likely to have missed certain extreme events.
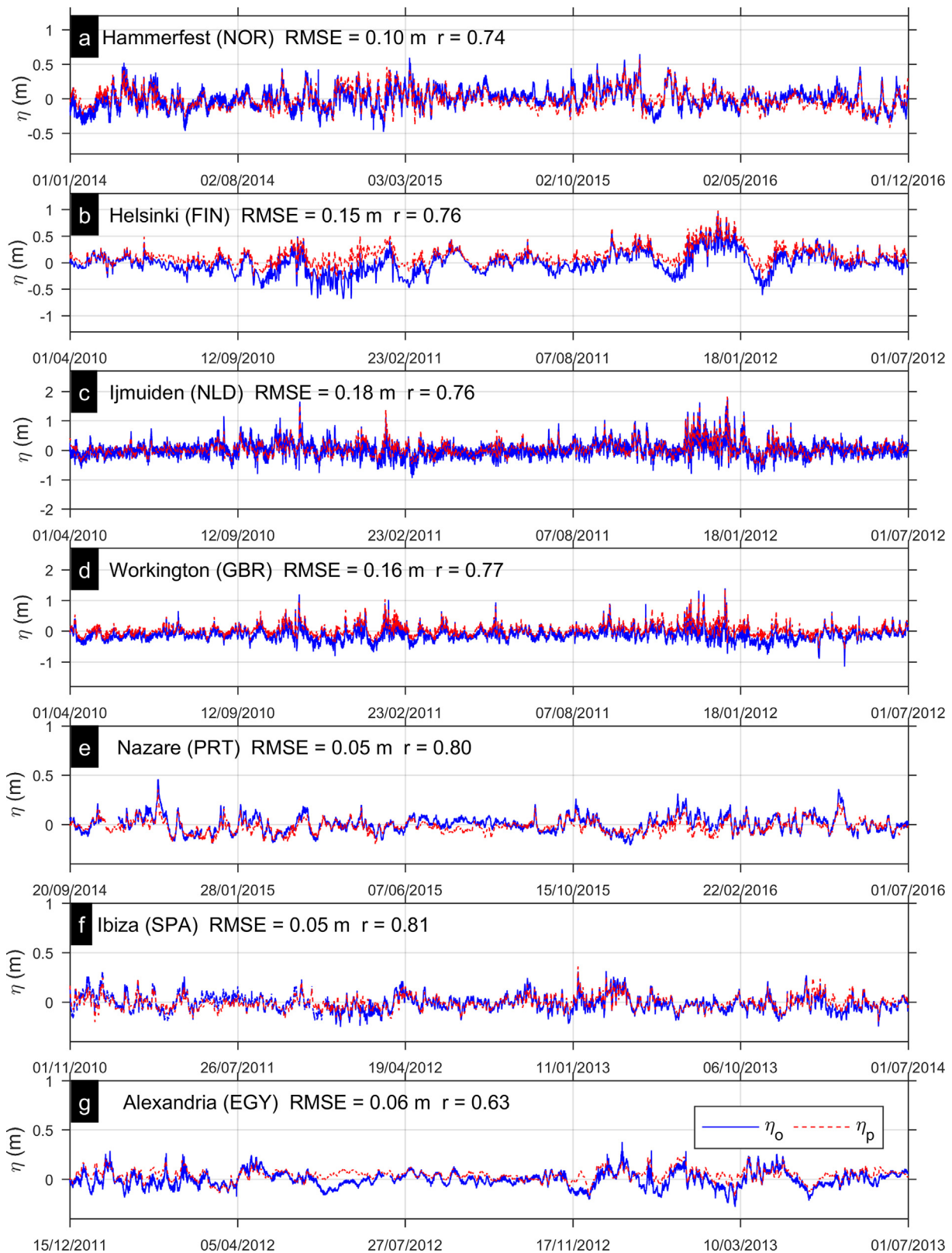
Fig. 2. Examples of comparisons of time series of simulated (red dashed line) and measured non-tidal residual (solid blue line) at seven tidal gauge stations representative of the different oceanographic areas. (For interpretation of the references to colour in this figure legend, the reader is referred to the web version of this article.)

The results show good agreement between the hindcast and the altimetry satellite NTR in the whole domain as demonstrated by the high skill scores (RMSE, and r). RMSE below 0.10 m is observed in the whole domain, with the exception of the southern coast of the North Sea and the Baltic Sea (Fig. 8a and Table 4) (RMSE ∼ 0.15 m). The RMSE along the Mediterranean Sea is around 0.07 m and RMSE
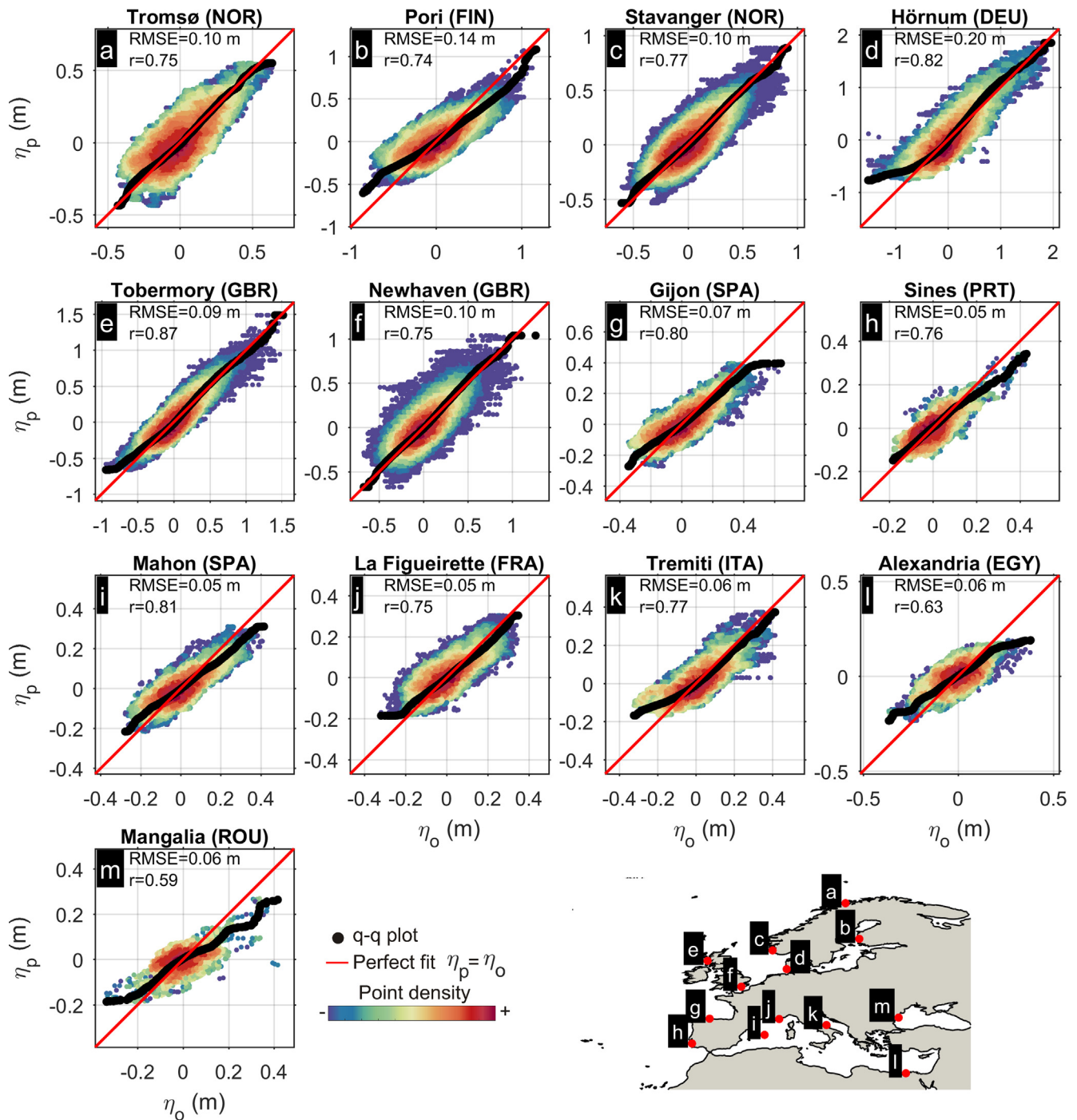
Fig. 3. Examples of scatter plots comparing measured and simulated non-tidal residual at different tidal gauge locations. The colours represent the point density increasing as they transition from blue to red. The black dots represent the quantile-quantile plot (q-q plot) while the red line indicates a perfect fit between observed and hindcast datasets. The inset map shows the locations of tide gauge stations. (For interpretation of the references to colour in this figure legend, the reader is referred to the web version of this article.)

values > = 0.05 m are characteristic of the southern S-North Atlantic, Iberian peninsula, Bay of Biscay and northern N-North Atlantic. RMSE < 0.07 m is observed in 70% of the 1° × 1° cells evaluated (Fig. 8b). Overall, %RMSE values fluctuate around 10–12% in at least 50% of the domain (Fig. 8c, Fig. 8d), with the %RMSE > 12% located in semi-enclosed basins (Baltic Sea, Mediterranean Sea and Black Sea). Regarding the time factor, values of 0.7 > r > 1 indicate the satisfactory performance of the hindcast (Fig. 8e, Fig. 8f). Values of r > 0.8 are present in over 50% of the whole domain. The spatial pattern of r is similar to the one of %RMSE variation, with lower

accuracy (r = 0.6) observed in semi-enclosed basins (Black Sea and Baltic Sea).

Overall, in terms of RMSE and r, the validation against satellite altimetry observations shows better performance than against tidal gauge measurements. However, the top %RMSE values are higher for the altimetry data validation. To notice that satellites have lower sampling frequency compared to ground stations, being constrained to the overpass interval and, consequentially, may not have captured some rare extreme events. The latter implies that the number of measurements of the altimetry data is lower than the one of tidal gauges,
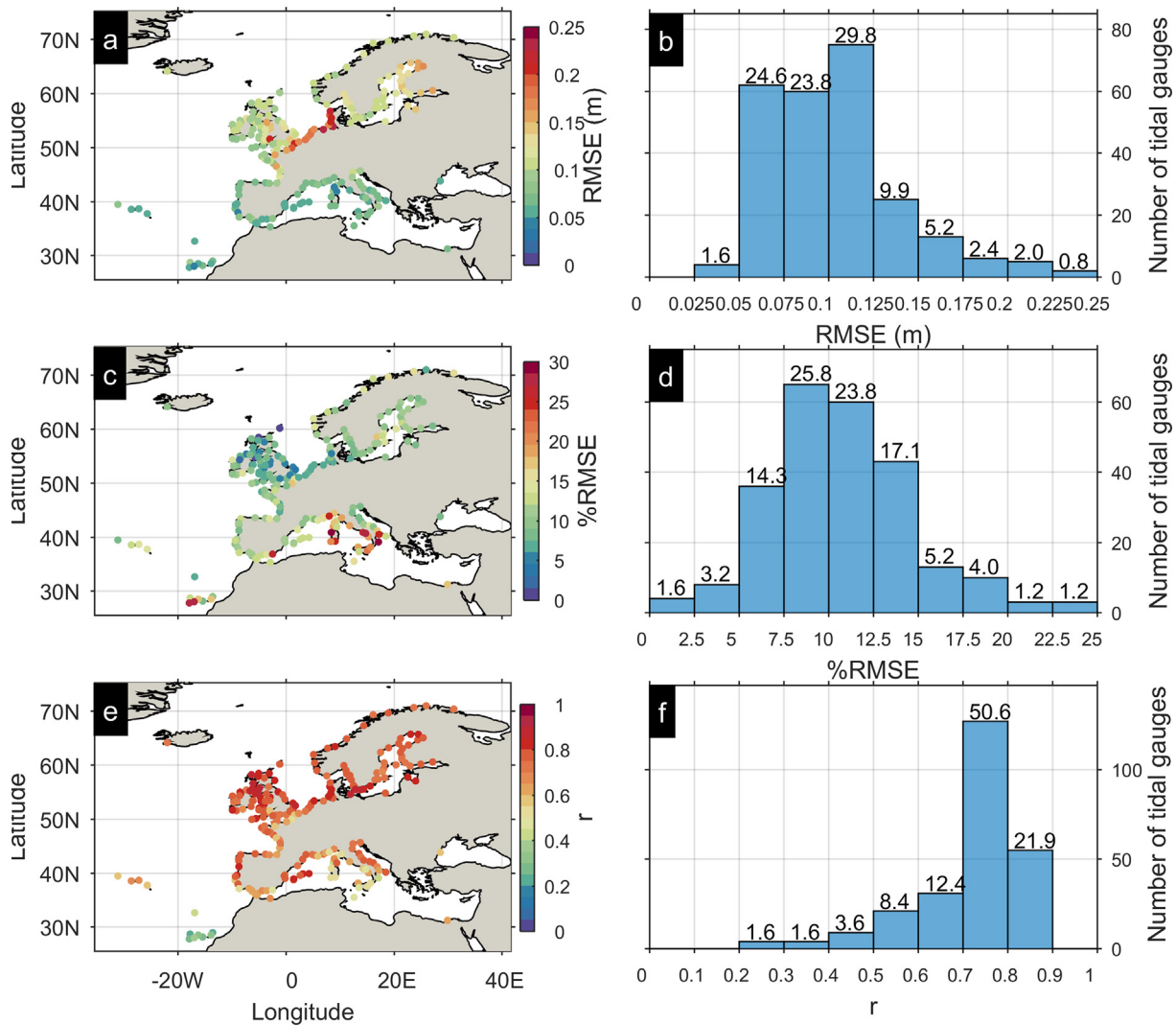
Fig. 4. Hindcast validation against tide gauge data. (a, c, e) Map scatter plots represent the RMSE, %RMSE and r; histograms (b, d, f) represent RMSE, %RMSE and r for all tidal gauges, where the vertical axis shows the count and the text labels above the bars the percentage of all tidal gauges belonging to the specific bin. (For interpretation of the references to colour in this figure legend, the reader is referred to the web version of this article.)

resulting in a higher %RMSE. Moreover, the ocean model omits processes contributing to sea surface height, like the steric ocean height driven by the thermo-steric and the halo-steric components that dominate the annual timescales in the Atlantic and Mediterranean Sea (Laiz et al., 2013). The steric height cycle has annual development/time scales and is well captured by satellite observation and further research is required to evaluate its contribution to extreme water levels.

Additionally, the current study conducted a validation of extreme SSL, via satellite observations, accounting only for the upper tail distribution (> 95th percentile). The results of the key statistic indexes (RMSE, %RMSE and correlation coefficient-r) are shown in Fig. 9 and Table 5. As expected, the upper tail RMSE (0.07 < RMSE < 0.40 m) is higher than the one obtained considering the whole time series (Fig. 9a). However, the hindcast shows a good representation of the

Table 2
Statistics of hindcast performance against non-tidal residual (NRT) measurements by tide gauge. Values are averaged along the defined ten European regions.

| Region	N Sta.	RMSE (m)					%RMSE (%)				r		
		Mean	Std	Min	Max	Mean	Std	Min	Max	Mean	Std	Min	Max
Black Sea	1	0.06	0.06	0.06	0.06	9	0	9	9	0.6	0.0	0.6	0.6
East Med.	1	0.06	0.06	0.06	0.06	17	0	17	17	0.6	0.0	0.6	0.6
Central Med.	31	0.07	0.01	0.05	0.10	17	7	8	30	0.6	0.1	0.4	0.8
West Med.	25	0.06	0.06	0.05	0.08	13	3	8	26	0.7	0.1	0.5	0.8
S-North Atlantic	24	0.07	0.06	0.04	0.10	13	5	7	28	0.6	0.2	0.2	0.8
Bay of Biscay	16	0.10	0.09	0.07	0.16	10	2	6	14	0.7	0.1	0.6	0.8
N-North Atlantic	52	0.11	0.10	0.08	0.20	8	3	1	17	0.8	0.1	0.5	0.9
North Sea	30	0.14	0.12	0.09	0.24	8	3	1	15	0.8	0.0	0.7	0.9
Baltic Sea	59	0.12	0.12	0.10	0.16	11	2	7	19	0.8	0.1	0.3	0.9
Norwegian Sea	10	0.11	0.10	0.10	0.12	12	3	7	16	0.8	0.0	0.7	0.8
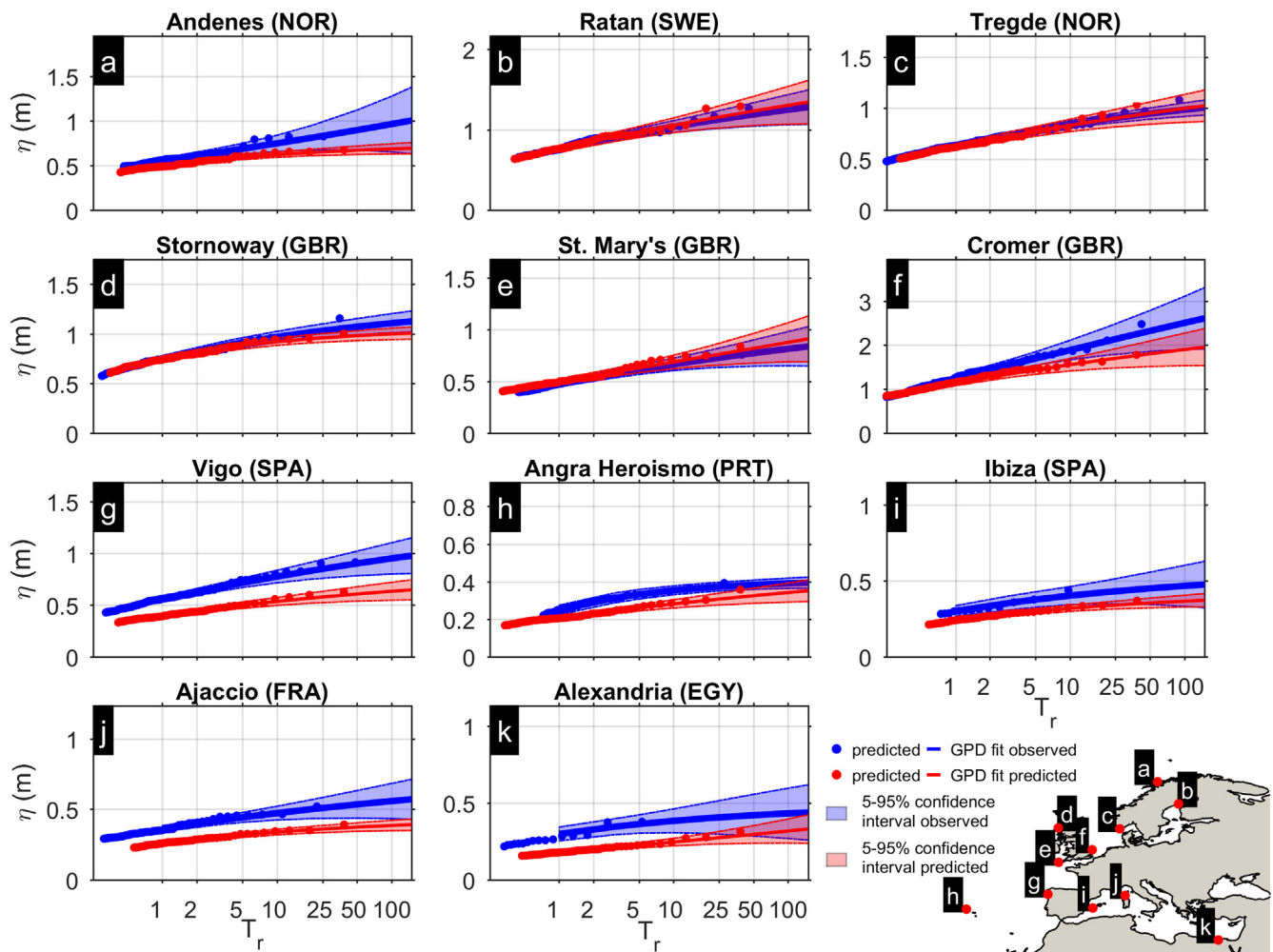
Fig. 5. Examples of extreme SSL validation results at selected tidal stations. The horizontal axis expresses the return period while the vertical axis shows the corresponding SSL. Dots represent the observed (blue) and modelled (red) extreme events, lines represent their GPD fitted probability distribution and the polygons the 5–95% confidence interval areas. The inset map shows the locations of the tide gauge stations. (For interpretation of the references to colour in this figure legend, the reader is referred to the web version of this article.)

extreme surge levels (RMSE < 0.12 m) along 73% of the study area (Fig. 9b). Higher RMSE values are detected along the Baltic Sea (> 0.2 m), the southern coast of the North Sea and the west coast of England (0.15–0.25 m). In those areas the error is mainly due to the under/overestimation of the upper/lower tail as indicates in Fig. 7. The %RMSE values are below 20% in almost 60% of the study area (Fig. 9c-d). %RMSE is higher in the Baltic Sea, Black Sea and East Mediterranean. The model also seems to satisfactorily reproduce the timing of extreme SSLs (r > 0.5) in 62% of the area, although r values are smaller compared to those calculated for the whole time series (especially in the Black Sea and East Mediterranean) (Fig. 9e–f).

3.3. Limitations

The main limitation of the ANYEU-SSL hindcast is the general tendency to underestimate the extreme storm surge levels. The above can have implications for potential applications related to hazard and risk assessments, especially in areas where BIAS RP10 exceeds 0.2 m. In those areas, the direct use of the dataset could result in an underestimation of the hazard, although it could be minimized by statistical correction using available time series of NTR, either from altimetry or tide gauges. The trend of underestimation is justified by (i) the fact that a continental model cannot resolve highly complex bathymetry features in shallow areas (Zijl et al., 2015) found at some parts of Europe; (ii) the

resolution of the atmospheric forcing also acts as a bottleneck in model skill, reducing the algorithm performance, especially in semi-enclosed basins (Fernández-Montblanc et al., 2019).

These constrains are exacerbated by the 2D approach used in our continental model. Two-dimensional models combine stability, computational efficiency, with reasonable accuracy, and therefore are the most common choice for storm surge prediction applications at large scale. However, 3D models can better reproduce the water level dynamics because they require less parameterization to reproduce all of the 3-D physical processes of water circulations (Lapetina and Sheng, 2015). Most of the above processes (sediment transport, coastal currents, wave-current boundary layers, vertical stratification, vertical varying wave induced circulation, wave induced forces, wave enhancement of bottom stress) take place nearshore and since they are related to wave processes, they require wave-coupling at a fine spatial resolution (in the order of tens of meters) (Bertin et al., 2015). These requirements could lead to very computational expensive setups which can be prohibitive for applications at a continental scale.

Sediment size and/or bed forms control bed roughness, thus turbulence and shear stress, both important factors for modelling of ocean circulation. In the absence of such information we assume a constant Manning coefficient, a choice which can affect the accuracy of the model. However, this is an inevitable assumption and alternatives like bottom friction enhancement using a varying Manning coefficient are
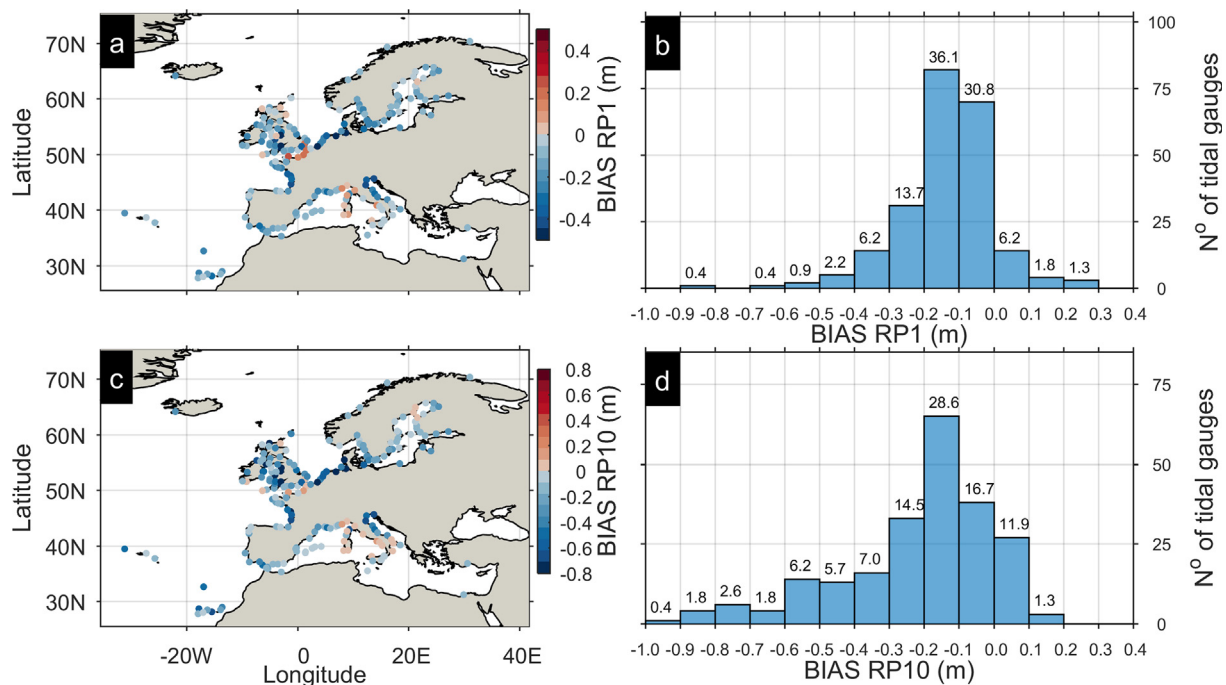
Fig. 6. Hindcast validation against tide gauges. Map of scatter plots of the absolute error of the 1-year (RP1) (a) and 10-year event (RP10) (b). Warm (cold) colours indicate that the hindcast overestimates (underestimates) extreme SSLs. (b, d) RP1, RP10 histograms for all tide gauges with the vertical axis showing the count and the text labels above the bars indicating the percentage of all tidal gauges belonging to the specific bin. (For interpretation of the references to colour in this figure legend, the reader is referred to the web version of this article.)

not granted to improve the model performance, as they cannot mimic all the complex physical processes (Lapetina and Sheng, 2015).

In summary, the performance of ANYEU-SSL comes with limitations related to the continental scale of the model. With the constantly increasing available computational power these inherent limitations can be gradually overcome using more complex modelling approaches (3D, waves, etc), following the examples of higher resolution regional models (Bertin et al., 2012; Lapetina and Sheng, 2015; Staneva et al., 2016; Wuxi et al., 2018). However, ANYEU-SSL does not aim to compete with such regional models, but aspires to provide a currently missing, long term hindcast dataset. Such a dataset can be particularly useful along areas where such information is not available, or can serve as boundary condition for regional-local models.

3.4. Trends in extreme SSLs along the European coastline

As a potential application of the ANYEU-SSL dataset we analyse the long-term trends along the European coastline, focussing on the yearly 10-year (Fig. 10a) and 100-year return level (Fig. 10b), for the period 1979–2016, expressed in mm per year (Fig. 10). The results indicate a

latitudinal gradient, with a moderate increase (< 5 mm/year) in extreme SSL observed in the southern area (< 50°N), and a decrease (> -5 mm/year) in the northern area (Fig. 10a-b). The N-North Atlantic area is the only high-latitude area where extreme SSLs appear to grow (> 5 mm/year), while the Azores and northern Azov Sea are the only southern areas where SSLs seem to be decreasing (< -5 mm/year). There is a drop of the extreme SSL in the German Bight and central area of the Norwegian Sea (10–15 mm/year for the 10-year return level and 5–10 mm/year for the 100-year return level). A notable reduction in extreme SSL (-10–20 mm/year) is found in the gulfs of Bothnia, Finland and Riga (Baltic Sea). On the contrary, extreme SSLs tend to increase (5–10 mm/year) in specific parts of the Central Mediterranean (eastern coast of Sardinia, Sicily, Northern Adriatic Sea) as well as along the eastern coast of the Black Sea.

The computed trends can locally differ from those calculated in previous studies. For example, Soomere and Pindsoo (2016) observed in the Baltic Sea opposite trends, with an increase in surge maxima for the period 1961–2004. Weisse et al. (2012) noticed no clear trends along the North Sea. On the contrary, in the southern area Cid et al. (2015) generally computed similar trends to the present ones, reporting storm

Table 3
Statistics of the hindcast skill to reproduce extreme storm surge levels, validated against tidal gauges. Values are averaged along the defined ten European regions.

|		BIAS RP1 (m)				BIAS RP10 (m)			
Region	N Sta.	Mean	Std	Min	Max	Mean	Std	Min	Max
Black Sea	–	–	–	–	–	–	–	–	–
East Med.	2	0.10	0.03	−0.12	−0.08	0.11	0.03	−0.14	−0.09
Central Med.	30	0.12	0.16	−0.43	0.15	0.17	0.25	−0.68	0.11
West Med.	25	0.12	0.06	−0.33	−0.06	0.15	0.10	−0.50	−0.01
S-North Atlantic	18	0.15	0.10	−0.33	−0.01	0.28	0.19	−0.71	−0.05
Bay of Biscay	14	0.23	0.12	−0.43	−0.03	0.32	0.22	−0.73	−0.05
N-North Atlantic	46	0.17	0.17	−0.65	0.23	0.33	0.31	−1.24	0.13
North Sea	25	0.19	0.22	−0.85	0.21	0.41	0.35	−1.45	0.08
Baltic Sea	60	0.13	0.07	−0.32	0.01	0.17	0.14	−0.56	0.10
Norwegian Sea	4	0.07	0.02	−0.09	−0.06	0.16	0.02	−0.17	−0.13
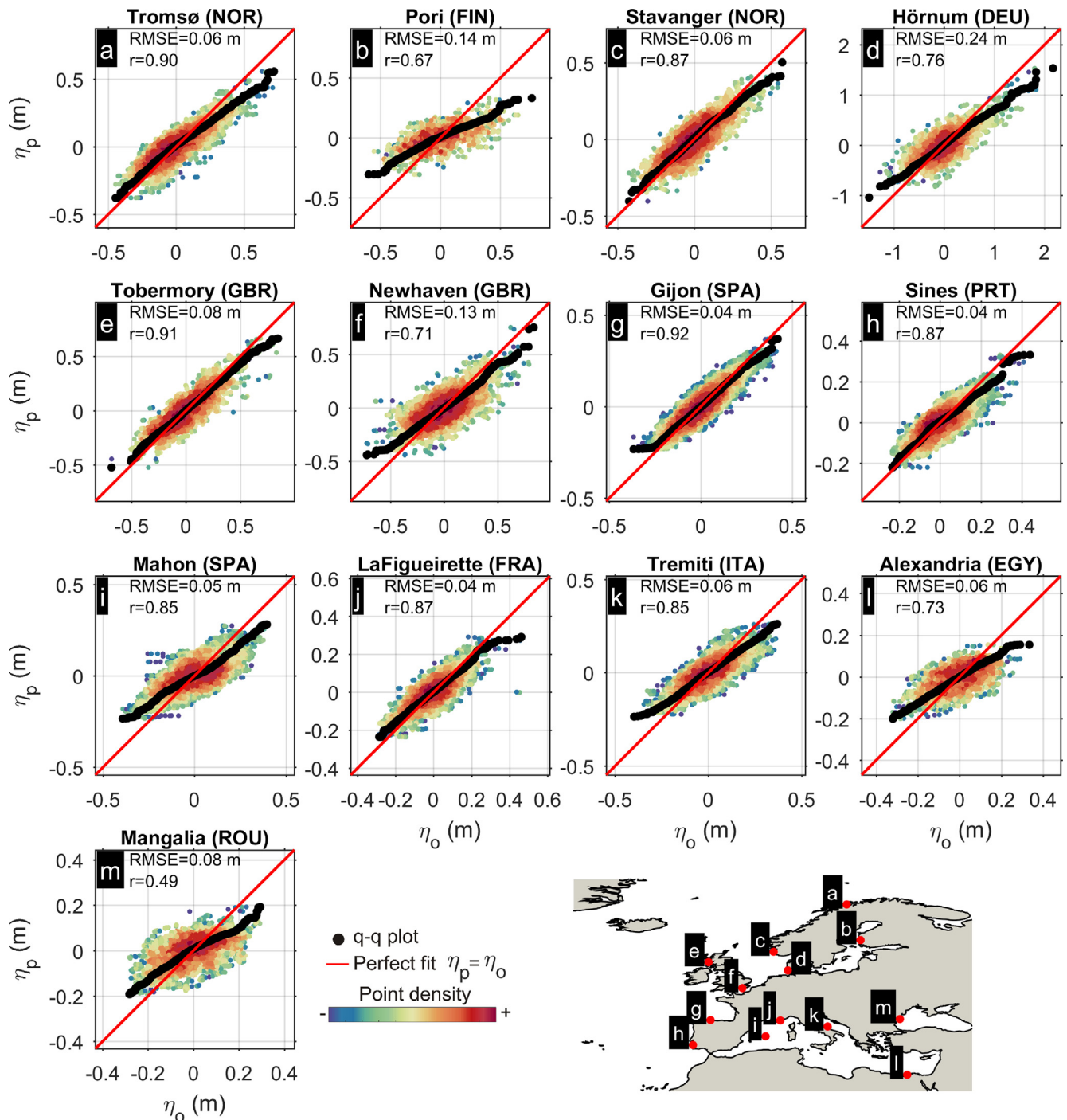
Fig. 7. Examples of scatter plots comparing altimetry measurements with simulated non-tidal residuals (NRT). The colours represent the point density, increasing as they transition from blue to red. The black dots represent the quantile-quantile plot (q-q plot) and the red line indicates the perfect fit between observed and hindcast dataset. The insert map shows the locations of tide gauges closest to the evaluated 1° × 1° cell. (For interpretation of the references to colour in this figure legend, the reader is referred to the web version of this article.)

surges increasing by 0–3 mm/year for the 1948–2013 period. Similarly, Makris et al. (2018) found a significantly increasing trend of annual storm surge extremes in the Mediterranean and Black Sea coastal zones for the 1979–2015 period. These major differences with respect to previous studies can be largely attributed to differences in the simulation period that was used by the previous authors (Calafat and Gomis, 2009; Cid et al., 2015). Indeed, extreme SSL shows considerable variation over time scales of decades and longer periods (Feng et al., 2018; Weisse et al., 2012) because of the changes in atmospheric circulation patterns. The public availability of a SSL dataset as ANYEU-SSL could

contribute to a better understanding of such dynamics. Likewise, the availability of different data sources can reduce the uncertainty of extreme SSL trends through cross-referencing among different databases.

The seasonal variability of the 100-year return level values is shown in Fig. 11. Overall, the seasonal spatial patterns follow the annual one (Fig. 10), although there are more coastal areas with no statistically significant seasonal trends. Likewise, depending on the season, opposite trends are observed in specific areas. In winter (Fig. 11a) a remarkable intensification of extreme SSL (10–15 mm/year) is recorded in Scotland and in the Bay of Liverpool (N-North Sea), while the opposite is
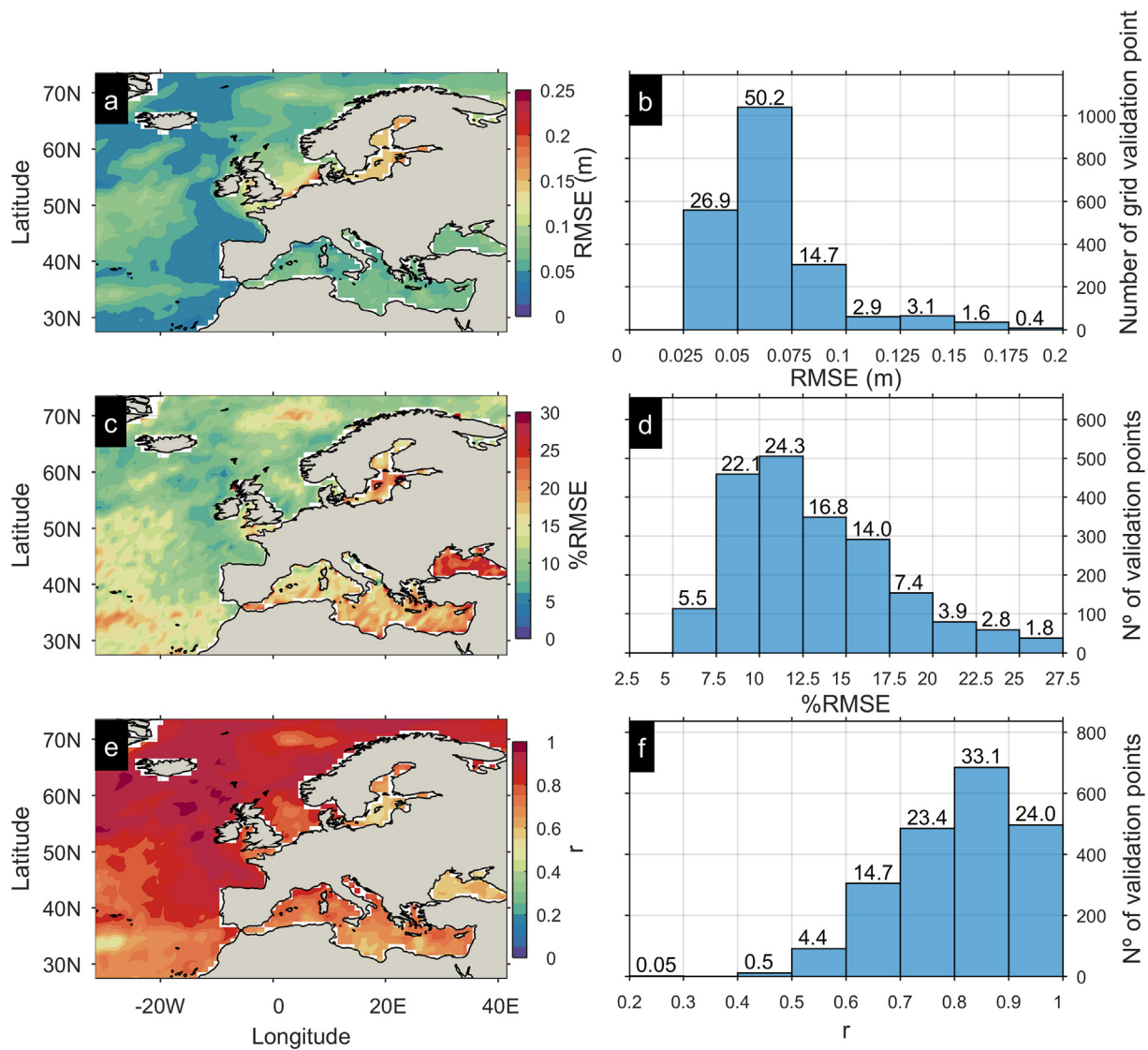
Fig. 8. Hindcast validation against satellite altimetry data. (a, c, e) Map scatter plots of RMSE, %RMSE and r; warm colours indicate higher performance; (b, d, f) RMSE, %RMSE and r histograms for all tidal gauges with the vertical axis showing the count and the text labels above the bars the percentage of all validation cells (1° × 1°) belonging to the specific bin. (For interpretation of the references to colour in this figure legend, the reader is referred to the web version of this article.)

Table 4
Statistics expressing the hindcast performance after comparison with the altimetry-observed non-tidal residual (NTR) along the defined ten European regions. N. Sta. indicates the number of 1° × 1°cells considered.

Region	RMSE (m)					%RMSE (%)				r		
	N. Sta.	Mean	Std	Min	Max	Mean	Std	Min	Max	Mean	Std	Min	Max
Black Sea	63	0.07	0.01	0.06	0.10	25	5	11	42	0.6	0.1	0.3	0.8
East Med.	103	0.07	0.01	0.05	0.10	20	4	12	29	0.7	0.1	0.6	0.8
Central Med.	134	0.06	0.01	0.05	0.09	18	4	6	32	0.7	0.1	0.5	0.8
West Med.	73	0.07	0.01	0.05	0.10	18	4	10	35	0.7	0.1	0.6	0.8
S-North Atlantic	367	0.05	0.01	0.03	0.10	14	3	8	28	0.7	0.1	0.5	0.9
Bay of Biscay	58	0.05	0.02	0.04	0.16	10	3	5	23	0.9	0.1	0.6	0.9
N-North Atlantic	479	0.06	0.02	0.04	0.26	10	3	6	30	0.9	0.1	0.4	1.0
North Sea	112	0.10	0.04	0.05	0.24	11	3	6	22	0.8	0.1	0.7	0.9
Baltic Sea	81	0.15	0.02	0.08	0.18	18	4	11	27	0.7	0.1	0.5	0.9
Norwegian Sea	147	0.08	0.02	0.05	0.21	12	3	7	27	0.9	0.1	0.5	0.9

observed on the west coast of the Iberian Peninsula. In spring opposite trends are observed (Fig. 11b): the extreme SSL increases on the west coast of German Bight (North Sea) (10–15 mm/year) and in the Gulf of Bothnia (5–10 mm/year). In addition, the general positive trend observed in the Withe Sea (Fig. 10) is reversed towards a decreasing extreme SSL (0–5 mm/year). In summer (Fig. 11c) an upward trend (2 mm/year) is observed in the Azores, while the Canary Islands and the west coast of northern Africa show negative trends. Finally an increase (5–10 mm/year) in autumn values is observed along the southern coast of the Baltic Sea and the Gulf of Bothnia (Fig. 11d).
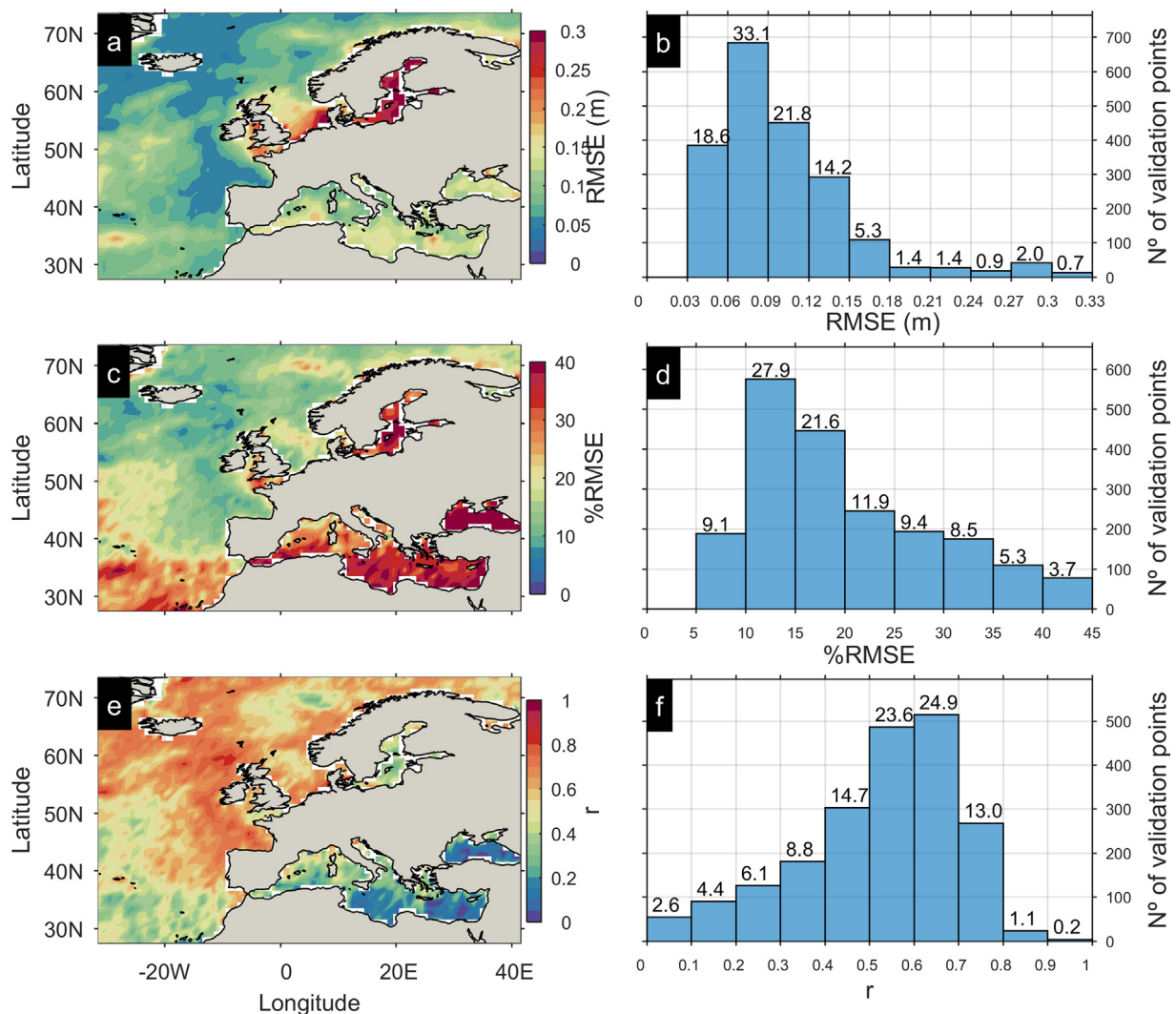
Fig. 9. Extreme SSL hindcast validation against satellite altimetry datasets (95th percentile). (a, c, e) Maps of scatter plots of RMSE, %RMSE and r; warm colours indicate higher performance; (b, d, f) RMSE, %RMSE and r histograms for all tidal gauges; the vertical axis shows the count and the text labels above the bars show the percentage of all validation cells (1° × 1°) belonging in the specific bin. (For interpretation of the references to colour in this figure legend, the reader is referred to the web version of this article.)

Table 5
Statistics of the extreme SSL validation (95th percentile) against altimetry data, along the defined ten European regions. N. Sta indicates the number of 1° × 1°cells considered.

Region	RMSE (m)					%RMSE (%)				r		
	N. Sta.	Mean	Std	Min	Max	Mean	Std	Min	Max	Mean	Std	Min	Max
Black Sea	52	0.14	0.02	0.11	0.24	43	6	25	53	0.1	0.1	−0.2	0.5
East Med.	89	0.13	0.02	0.08	0.21	36	5	25	48	0.2	0.1	−0.1	0.4
Central Med.	116	0.12	0.02	0.07	0.16	31	7	11	44	0.3	0.1	0.0	0.7
West Med.	62	0.12	0.03	0.07	0.18	30	7	16	45	0.4	0.1	0.1	0.6
S-North Atlantic	363	0.08	0.02	0.05	0.20	23	7	10	42	0.5	0.1	0.0	0.8
Bay of Biscay	53	0.07	0.02	0.05	0.18	13	4	7	30	0.7	0.1	0.5	0.8
N-North Atlantic	449	0.08	0.04	0.04	0.26	13	4	7	36	0.6	0.1	0.3	0.8
North Sea	103	0.16	0.07	0.07	0.40	16	3	9	24	0.6	0.1	0.5	0.8
Baltic Sea	59	0.28	0.04	0.14	0.36	34	8	18	51	0.5	0.1	0.2	0.8
Norwegian Sea	132	0.12	0.03	0.07	0.20	18	3	10	26	0.6	0.1	0.4	0.7

Seasonal trends of extreme storm surge are significant, since they can increase the likelihood of compound risk related to flooding and erosion. For instance, such variation in seasonal trends could increase the probability of a conjunction of an extreme storm surge and a flooding caused by river discharge or high precipitation (Bevacqua et al., 2019; Paprotny et al., 2018). In this regard, the present dataset provides continuous and high temporal and spatial resolution sources to aid this kind of research.

4. Conclusions

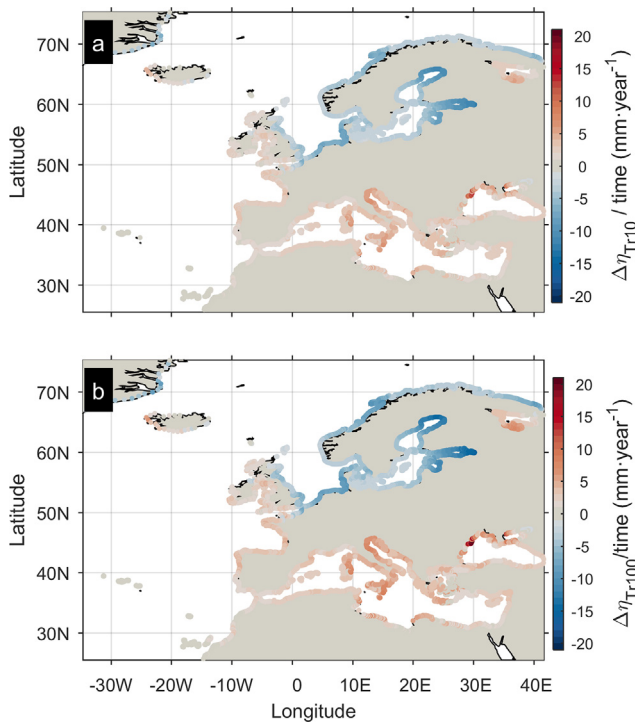This contribution presents a high-resolution Pan-European storm

Fig. 10. Trends of extreme storm surge levels along the European coastline for the period 1979–2016. (a) Is the linear trend of the annual mean 10-year and (b) is the 100-year return level value. Warm (cold) colours indicate an increase (decrease) in the magnitude of the extreme storm surge level (only values with p < 0.05 are shown in the figure). (For interpretation of the references to colour in this figure legend, the reader is referred to the web version of this article.)

surge dataset, ANYEU-SSL, produced with the SCHISM circulation model. The dataset covers 40 years (1979–2018) of SSL data along the European coastline with a 3-hour temporal resolution.
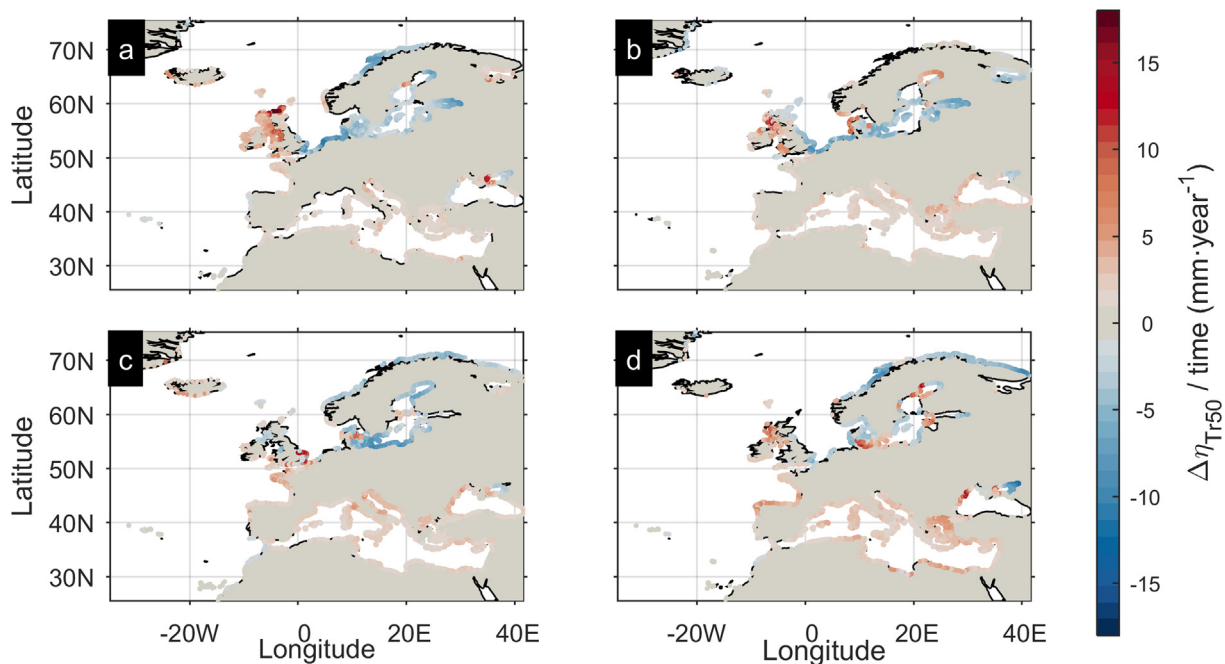
The ANYEU-SSL dataset has been extensively validated for the period 1992–2016, considering the whole time series, as well as only extreme SSL values. In shallow water the hindcast results were evaluated against sea level measurements from 252 tide gauges distributed along the whole European coastline. At the open sea, ANYEU-SSL was compared with SSL measurements obtained via satellite altimetry covering the entire modelling domain. The results indicate a satisfactory skill to reproduce the NTR and extreme SSLs along the European coastline, in terms of both timing and magnitude. When validating against tide gauges, the whole hindcast (NTR) shows a mean RMSE of 0.10 m for Europe, while 50% and 75% of the tidal stations show RMSE of 0.7 m and 0.12 m, respectively. The RMSE is below 0.07 m in 75% of the area evaluated using satellite altimetry. A relative decrease in the hindcast performance is observed in the case of extreme SSL validation. Considering only the extremes, the validation against tide gauges shows that the model tends to underestimate extreme SSLs, with RMSE for the 1 and 10-year events being −0.13 and −0.23. The comparison of extreme SSLs with satellite altimetry measurements in the open ocean shows an average RMSE of 0.10 m, whereas the 25th and 75th percentiles of RMSE ranges from 0.06 to 0.12 m. Overall, the hindcast shows a trend to underestimate extreme SSLs. The above implies that, being a continental scale dataset, ANYEU SSL should be used with caution, especially at local scale; e.g. for detailed coastal hazard and risk assessments. In those cases the underestimated extreme SSLs can result in lower estimates of risk. However, this is a known weakness of large-scale models, the main advantage of which is that they resolve the spatio-temporal SSL dynamics in a homogenized framework.

ANYEU-SSL provides uniform information on a Pan-European scale, and as an application example, we did an analysis of the spatial and temporal variability of extreme storm surge trends. Results show an overall latitudinal gradient in the trend of the extreme storm surge magnitude for the studied period (1979–2016), increasing in latitude > 50° N and diminishing the extreme SSL magnitude in latitude < 50°. Additionally, a strong seasonal variation of extreme SSLs was observed in the northern areas.

Fig. 11. Seasonal trends of the yearly 100-year return level along the European coastline for the period 1979–2016. (a) Winter (from December to February DJF). (b) Spring (from March to May). (c) Summer (from June to August). (d) Autumn (from September to November); warm colours indicate increases in the magnitude of the extreme storm surge level (only values with p < 0.05 shown in the figure). (For interpretation of the references to colour in this figure legend, the reader is referred to the web version of this article.)
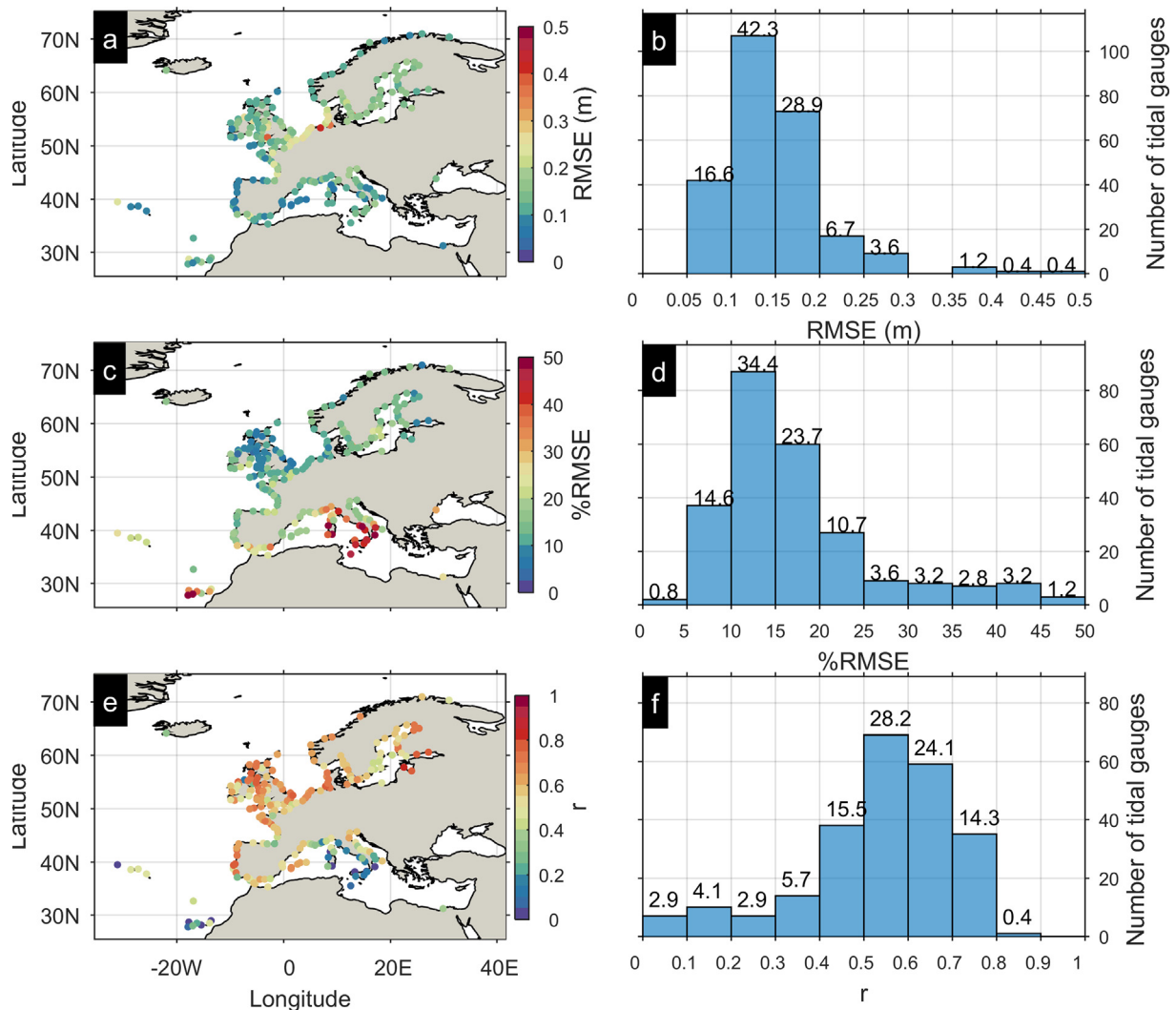
Fig. A1. Extreme SSL hindcast validation results against tidal gauge data (95th percentile). (a, c, e) Map scatter plots of RMSE, %RMSE and r respectively; (b, d, f) RMSE, %RMSE and r histograms for all tidal gauges where the vertical axis shows the count and the text labels above the bars the percentage of all tidal gauges belonging in the specific bin.

Acknowledgments

Appendix A

See Fig. A1

Appendix B. Supplementary material

Supplementary data to this article can be found online at https://doi.org/10.1016/j.envint.2019.105367.

References

Androulidakis, Y.S., Kombiadou, K.D., Makris, C.V., Baltikas, V.N., Krestenitis, Y.N., 2015. Storm surges in the Mediterranean Sea: Variability and trends under future climatic conditions. Dyn. Atmos. Ocean. 71, 56–82. https://doi.org/10.1016/j.dynatmoce.2015.06.001.

Bamber, J.L., Oppenheimer, M., Kopp, R.E., Aspinall, W.P., Cooke, R.M., 2019. Ice sheet contributions to future sea-level rise from structured expert judgment. Proc. Natl. Acad. Sci. 116, 11195–11200. https://doi.org/10.1073/PNAS.1817205116.

Bertin, X., Bruneau, N., Breilh, J.-F., Fortunato, A.B., Karpytchev, M., 2012. Importance of wave age and resonance in storm surges: The case Xynthia. Bay of Biscay. Ocean Model. 42, 16–30. https://doi.org/10.1016/j.ocemod.2011.11.001.

Bertin, X., Li, K., Roland, A., Bidlot, J.-R., 2015. The contribution of short-waves in storm surges: Two case studies in the Bay of Biscay. Cont. Shelf Res. 96, 1–15. https://doi.org/10.1016/j.csr.2015.01.005.

Bertin, X., Prouteau, E., Letetrel, C., 2013. A significant increase in wave height in the North Atlantic Ocean over the 20th century. Glob. Planet. Change 106, 77–83. https://doi.org/10.1016/J.GLOPLACHA.2013.03.009.

Bevacqua, E., Maraun, D., Vousdoukas, M.I., Voukouvalas, E., Vrac, M., Mentaschi, L., Widmann, M., 2019. Higher probability of compound flooding from precipitation and storm surge in Europe under anthropogenic climate change. Sci. Adv. 5, eaaw5531. https://doi.org/10.1126/sciadv.aaw5531.

Butler, A., Heffernan, J.E., Tawn, J.A., Flather, R.A., Horsburgh, K.J., 2007. Extreme value analysis of decadal variations in storm surge elevations. J. Mar. Syst. 67, 189–200. https://doi.org/10.1016/j.jmarsys.2006.10.006.

Calafat, F.M., Avgoustoglou, E., Jordà, G., Flocas, H., Zodiatis, G., Tsimplis, M.N., Kouroutzoglou, J., 2014. The ability of a barotropic model to simulate sea level

extremes of meteorological origin in the Mediterranean Sea, including those caused by explosive cyclones. J. Geophys. Res. Ocean. 119, 7840–7853. https://doi.org/10.1002/2014JC010360.

Calafat, F.M., Gomis, D., 2009. Reconstruction of Mediterranean sea level fields for the period 1945–2000. Glob. Planet. Change 66, 225–234. https://doi.org/10.1016/j.gloplacha.2008.12.015.

Camus, P., Mendez, F.J., Medina, R., Tomas, A., Izaguirre, C., 2013. High resolution downscaled ocean waves (DOW) reanalysis in coastal areas. Coast. Eng. 72, 56–68. https://doi.org/10.1016/J.COASTALENG.2012.09.002.

Chawla, A., Spindler, D.M., 2013. Validation of a thirty year wave hindcast using the Climate Forecast System Reanalysis winds. Ocean Model. 70, 189–206. https://doi.org/10.1016/J.OCEMOD.2012.07.005.

Cid, A., Castanedo, S., Abascal, A.J., Menéndez, M., Medina, R., 2014. A high resolution hindcast of the meteorological sea level component for Southern Europe: the GOS dataset. Clim. Dyn. 43, 2167–2184. https://doi.org/10.1007/s00382-013-2041-0.

Cid, A., Menéndez, M., Castanedo, S., Abascal, A.J., Méndez, F.J., Medina, R., 2015. Long-term changes in the frequency, intensity and duration of extreme storm surge events in southern Europe. Clim. Dyn. 46, 1503–1516. https://doi.org/10.1007/s00382-015-2659-1.

Cipollini, P., Calafat, F.M., Jevrejeva, S., Melet, Angelique, M., Prandi, P., 2017. Monitoring Sea Level in the Coastal Zone with Satellite Altimetry and Tide Gauges. Surv. Geophys. 38, 33–57. https://doi.org/10.1007/s10712-016-9392-0.

Conte, D., Lionello, P., 2013. Characteristics of large positive and negative surges in the Mediterranean Sea and their attenuation in future climate scenarios. Glob. Planet. Change 111, 159–173. https://doi.org/10.1016/J.GLOPLACHA.2013.09.006.

Dangendorf, S., Muler-Navarra, S., Jensen, J., Schenk, F., Wahl, T., Weisse, R., 2014. North sea storminess from a novel storm surge record since AD 1843. J. Clim. 27, 3582–3595. https://doi.org/10.1175/jcli-d-13-00427.1.

Elsner, J., Kossin, J.P., Jagger, T.H., 2008. The increasing intensity of the strongest tropical cyclones. Nature 455, 92. https://doi.org/10.1038/nature07234.

Feng, J., Li, D., Li, Y., Liu, Q., Wang, A., 2018. Storm surge variation along the coast of the Bohai Sea. Sci. Rep. 8, 11309. https://doi.org/10.1038/s41598-018-29712-z.

Fernández-Montblanc, T., Vousdoukas, M.I., Ciavola, P., Voukouvalas, E., Mentaschi, L., Breyiannis, G., Feyen, L., Salamon, P., 2019. Towards robust pan-European storm surge forecasting. Ocean Model. 133, 129–144. https://doi.org/10.1016/j.ocemod.2018.12.001.

Fortunato, A., Li, K., Bertin, X., Rodrigues, M., Martin Miguez, B., 2016. Determination of extreme sea levels along the Iberian Atlantic coast. Ocean Eng. 111, 471–482. https://doi.org/10.1016/j.oceaneng.2015.11.031ï.

Haigh, I.D., Wadey, M.P., Wahl, T., Ozsoy, O., Nicholls, R.J., Brown, J.M., Horsburgh, K., Gouldby, B., 2016. Spatial and temporal analysis of extreme sea level and storm surge events around the coastline of the UK. Scientific Data 3, 160107. https://doi.org/10.1038/sdata.2016.107.

Hamon, M., Beuvier, J., Somot, S., Lellouche, J.-M., Greiner, E., Jordà, G., Bouin, M.-N., Arsouze, T., Béranger, K., Sevault, F., Dubois, C., Drevillon, M., Drillet, Y., 2016. Design and validation of MEDRYS, a Mediterranean Sea reanalysis over the period 1992–2013. Ocean Sci. 12, 577–599. https://doi.org/10.5194/os-12-577-2016.

Hatzikyriakou, A., Lin, N., 2017. Simulating storm surge waves for structural vulnerability estimation and flood hazard mapping. Nat. Hazards 89, 939–962. https://doi.org/10.1007/s11069-017-3001-5.

Hemer, M.A., Fan, Y., Mori, N., Semedo, A., Wang, X.L., 2013. Projected changes in wave climate from a multi-model ensemble. Nat. Clim. Chang. 3, 471–476. https://doi.org/10.1038/nclimate1791.

Hinkel, J., Lincke, D., Vafeidis, A.T., Perrette, M., Nicholls, R.J., Tol, R.S.J., Marzeion, B., Fettweis, X., Ionescu, C., Levermann, A., 2014. Coastal flood damage and adaptation costs under 21st century sea-level rise. Proc. Natl. Acad. Sci. USA 111, 3292–3297. https://doi.org/10.1073/pnas.1222469111.

Jevrejeva, S., Jackson, L.P., Riva, R.E.M., Grinsted, A., Moore, J.C., 2016. Coastal sea level rise with warming above 2 °C. Proc. Natl. Acad. Sci. USA 113, 13342–13347. https://doi.org/10.1073/pnas.1605312113.

Jordà, G., Gomis, D., Álvarez-Fanjul, E., 2012. The VANI2-ERA hindcast of sea-level residuals: atmospheric forcing of sea-level variability in the Mediterranean Sea (1958–2008). Sci. Mar. 76, 133–146. https://doi.org/10.3989/scimar.03612.19C.

Laiz, I., Gómez-Enri, J., Tejedor, B., Aboitiz, A., Villares, P., 2013. Seasonal sea level variations in the gulf of Cadiz continental shelf from in-situ measurements and satellite altimetry. Cont. Shelf Res. 53, 77–88. https://doi.org/10.1016/J.CSR.2012.12.008.

Lapetina, A., Sheng, Y.P., 2015. Simulating complex storm surge dynamics: Three-dimensionality, vegetation effect, and onshore sediment transport. J. Geophys. Res. Ocean. 120, 7363–7380. https://doi.org/10.1002/2015JC010824.

Makris, C., Androulidakis, Y., Baltikas, V., Krestenitis, Y., 2018. A 37-year analysis of the storm surges in the Mediterranean and Black Seas, in: 12th Panhellenic Symposium of Oceanography and Fisheries. Corfu, Greece, p. 14.

Marcos, M., Jordà, G., Gomis, D., Pérez, B., 2011. Changes in storm surges in southern Europe from a regional model under climate change scenarios. Glob. Planet. Change 77, 116–128. https://doi.org/10.1016/J.GLOPLACHA.2011.04.002.

Meier, H.E.M., 2006. Baltic Sea climate in the late twenty-first century: a dynamical downscaling approach using two global models and two emission scenarios. Clim. Dyn. 27, 39–68. https://doi.org/10.1007/s00382-006-0124-x.

Menendez, M., García-Díez, M., Fita, L., Fernández, J., Méndez, F.J., Gutiérrez, J.M., 2014. High-resolution sea wind hindcasts over the Mediterranean area. Clim. Dyn. 42, 1857–1872. https://doi.org/10.1007/s00382-013-1912-8.

Menéndez, M., Woodworth, P.L., 2010. Changes in extreme high water levels based on a quasi-global tide-gauge data set. J. Geophys. Res 115, C10011. https://doi.org/10.1029/2009JC005997.

Mentaschi, L., Vousdoukas, M., Voukouvalas, E., Sartini, L., Feyen, L., Besio, G., Alfieri, L.,

2016. The transformed-stationary approach: a generic and simplified methodology for non-stationary extreme value analysis. Hydrol. Earth Syst. Sci. 20, 3527–3547. https://doi.org/10.5194/hess-20-3527-2016.

Muis, S., Verlaan, M., Nicholls, R.J., Brown, S., Hinkel, J., Lincke, D., Vafeidis, A.T., Scussolini, P., Winsemius, H.C., Ward, P.J., 2017. A comparison of two global datasets of extreme sea levels and resulting flood exposure. Earth's Futur. 5, 379–392. https://doi.org/10.1002/2016EF000430.

Muis, S., Verlaan, M., Winsemius, H.C., Aerts, J.C.J.H., Ward, P.J., 2016. A global reanalysis of storm surges and extreme sea levels. Nat. Commun. 7, 11969. https://doi.org/10.1038/ncomms11969 | www.nature.com/naturecommunications.

Oumeraci, H., 1994. Review and analysis of vertical breakwater failures — lessons learned. Coast. Eng. 22, 3–29. https://doi.org/10.1016/0378-3839(94)90046-9.

Paprotny, D., Morales-Napoles, O., Nikulin, G., 2016. Extreme sea levels under present and future climate: a pan-European database. E3S Web Conf. 7. https://doi.org/10.1051/e3sconf/20160702001.

Paprotny, D., Vousdoukas, M.I., Morales-Nápoles, O., Jonkman, S.N., Feyen, L., 2018. Compound flood potential in Europe. Hydrol. Earth Syst. Sci. Discuss. 1–34. https://doi.org/10.5194/hess-2018-132.

Pawlowicz, R., Beardsley, B., Lentz, S., 2002. Classical tidal harmonic analysis including error estimates in MATLAB using T_TIDE. Comput. Geosci. 28, 929–937. https://doi.org/10.1016/S0098-3004(02)00013-4.

Pond, S., Pickard, G.L., 2013. Introductory dynamical oceanography. Elsevier, Amsterdam, The Netherlands.

Ratsimandresy, A.W., Sotillo, M.G., Carretero Albiach, J.C., Álvarez Fanjul, E., Hajji, H., 2008. A 44-year high-resolution ocean and atmospheric hindcast for the Mediterranean Basin developed within the HIPOCAS Project. Coast. Eng. 55, 827–842. https://doi.org/10.1016/J.COASTALENG.2008.02.025.

Resio, D.T., Westerink, J.J., 2008. Modeling the physics of storm surges. Phys. Today 61, 33–38. https://doi.org/10.1063/1.2982120.

Sebastião, P., Guedes Soares, C., Alvarez, E., 2008. 44 years hindcast of sea level in the Atlantic Coast of Europe. Coast. Eng. 55, 843–848. https://doi.org/10.1016/j.coastaleng.2008.02.022.

Shaw, A., Hashemi, M.R., Spaulding, M., Oakley, B., Baxter, C., 2016. Effect of coastal erosion on storm surge: A case study in the southern coast of Rhode Island. J. Mar. Sci. Eng. 4. https://doi.org/10.3390/jmse4040085.

Smith, A.M., Mather, A.A., Bundy, S.C., Cooper, J.A.G., Guastella, L.A., Ramsay, P.J., Theron, A., 2010. Contrasting styles of swell-driven coastal erosion: Examples from KwaZulu-Natal, South Africa. Geol. Mag. 147, 940–953. https://doi.org/10.1017/S0016756810000361.

Soomere, T., Pindsoo, K., 2016. Spatial variability in the trends in extreme storm surges and weekly-scale high water levels in the eastern Baltic Sea. Cont. Shelf Res. 115, 53–64. https://doi.org/10.1016/J.CSR.2015.12.016.

Spencer, T., Brooks, S.M., Evans, B.R., Tempest, J.A., Möller, I., 2015. Southern North Sea storm surge event of 5 December 2013: Water levels, waves and coastal impacts. Earth-Science Rev. 146, 120–145. https://doi.org/10.1016/j.earscirev.2015.04.002.

Staneva, J., Wahle, K., Günther, H., Stanev, E., 2016. Coupling of wave and circulation models in coastal–ocean predicting systems: a case study for the German Bight. Ocean Sci. 12, 797–806. https://doi.org/10.5194/os-12-797-2016.

Tsimplis, M.N., Blackman, D., 1997. Extreme sea-level distribution and return periods in the aegean and ionian seas Estuarine. Coastal Shelf Sci. 44, 79–89. https://doi.org/10.1006/ecss.1996.0126.

Vousdoukas, M.I., Mentaschi, L., Voukouvalas, E., Bianchi, A., Dottori, F., Feyen, L., 2018a. Climatic and socioeconomic controls of future coastal flood risk in Europe. Nat. Clim. Chang. https://doi.org/10.1038/s41558-018-0260-4.

Vousdoukas, M.I., Mentaschi, L., Voukouvalas, E., Verlaan, M., Feyen, L., 2017. Extreme sea levels on the rise along Europe's coasts. Earth's Future 5 (3), 304–323. https://doi.org/10.1002/2016EF000505.

Vousdoukas, M.I., Mentaschi, L., Voukouvalas, E., Verlaan, M., Jevrejeva, S., Jackson, L.P., Feyen, L., 2018b. Global probabilistic projections of extreme sea levels show intensification of coastal flood hazard. Nat. Commun. 9, 2360. https://doi.org/10.1038/s41467-018-04692-w.

Wahl, T., Haigh, I.D., Nicholls, R.J., Arns, A., Dangendorf, S., Hinkel, J., Slangen, A.B.A., 2017. Understanding extreme sea levels for broad-scale coastal impact and adaptation analysis. Nat. Commun. 8, 16075. https://doi.org/10.1038/ncomms16075.

Weidemann, H., 2015. coastDat-2 TRIM-NP-2d-Baltic_Sea. https://doi.org/10.1594/WDCC/coastDat-2_TRIM-NP-2d-Baltic.

Weisse, R., von Storch, H., Niemeyer, H.D., Knaack, H., 2012. Changing North Sea storm surge climate: An increasing hazard? Ocean Coast Manag. 68, 58–68. https://doi.org/10.1016/J.OCECOAMAN.2011.09.005.

Woth, K., Weisse, R., von Storch, H., 2006. Climate change and North Sea storm surge extremes: an ensemble study of storm surge extremes expected in a changed climate projected by four different regional climate models. Ocean Dyn. 56, 3–15. https://doi.org/10.1007/s10236-005-0024-3.

Wuxi, Q., Li, J., Nie, B., 2018. Effects of tide-surge interaction and wave set-up/set-down on surge: case studies of tropical cyclones landing China's Zhe-Min coast. Theor. Appl. Mech. Lett. 8, 153–159. https://doi.org/10.1016/j.taml.2018.03.002.

Zhang, Y., Baptista, A.M., 2008. SELFE: A semi-implicit Eulerian-Lagrangian finite-element model for cross-scale ocean circulation. Ocean Model. 21, 71–96. https://doi.org/10.1016/J.OCEMOD.2007.11.005.

Zhang, Y.J., Ye, F., Stanev, E.V., Grashorn, S., 2016. Seamless cross-scale modeling with SCHISM. Ocean Model. 102, 64–81. https://doi.org/10.1016/J.OCEMOD.2016.05.002.

Zijl, F., Sumihar, J., Verlaan, M., 2015. Application of data assimilation for improved operational water level forecasting on the northwest European shelf and North Sea. Ocean Dyn. 65, 1699–1716. https://doi.org/10.1007/s10236-015-0898-7.